

Morphology of a quantum catastrophe

J. Mumford, E. Turner, D. W. L. Sprung, and D. H. J. O'Dell
*Department of Physics and Astronomy, McMaster University,
 1280 Main St. W., Hamilton, ON, L8S 4M1, Canada*
 (Dated: October 26, 2016)

Thom's seven elementary catastrophes are the only structurally stable singularities in up to four dimensions [1]. Their stability against perturbations removes any symmetry requirement which accounts for their ubiquity in nature, e.g. as caustics. Examples include rainbows [2], the twinkling of starlight [3], rogue waves at sea [4] and structure formation in the universe [5]. At large scales the intensity appears to diverge on a caustic, but at the scale of a wavelength interference smooths the singularity and produces characteristic diffraction patterns [6–9]. At subwavelength scales wave catastrophes are organized by an underlying lattice of dislocations (nodes) around each of which the wave function circulates as a vortex [10, 11]. Here we study the morphology of a third generation beyond geometric and wave catastrophes, called quantum catastrophes, which are singularities of classical fields. They are regulated by quantizing the excitations, i.e. second quantization [12–15], and live in Fock space which, being fundamentally discrete, leads to core-less discretized vortices. These are created or annihilated in pairs as the number of quanta is varied.

A famous example of the necessity of quantizing excitations is Planck's spectrum which avoids the ultraviolet catastrophe by treating the electromagnetic field in terms of discrete energy units: photons. The term 'quantum catastrophe' was coined by Leonhardt [12] to describe the phase singularity suffered by a classical wave passing an event horizon: in quantum field theory pairs of photons are emitted as Hawking radiation. In this letter we examine catastrophes in a simple field composed of just two modes. Physical examples include the two polarization states of photons in a laser beam [16, 17], the Lipkin-Meshkov-Glick model in nuclear physics [18], the Ising model with infinite range interactions [19], and two coupled Bose-Einstein condensates (BECs) forming a Josephson junction [20–22].

Consider a bosonic field with two modes and the associated annihilation operators \hat{a}_0 and \hat{a}_1 . If there are N excitations the problem can be mapped onto a quantum spin of length $N/2$ using the Schwinger representation $\hat{S}_x = (\hat{a}_1^\dagger \hat{a}_0 + \hat{a}_0^\dagger \hat{a}_1)/2$, $\hat{S}_y = i(\hat{a}_1^\dagger \hat{a}_0 - \hat{a}_0^\dagger \hat{a}_1)/2$ and $\hat{S}_z = (\hat{a}_1^\dagger \hat{a}_1 - \hat{a}_0^\dagger \hat{a}_0)/2$ [23]. Choosing the z basis, the quantum state of the field $|\psi\rangle = \sum a_z |z\rangle$ is fully specified by the amplitudes a_z of the Fock states $|z\rangle$ which correspond to the discrete difference in the number of excitations between the two modes. It is convenient to define $z = (N_1 - N_0)/N = 2S_z/N$, so that z takes values between -1 and +1 in steps of $1/N$.

Dynamics are obtained by evolving with a Hamiltonian. For example, the two-site Bose-Hubbard model

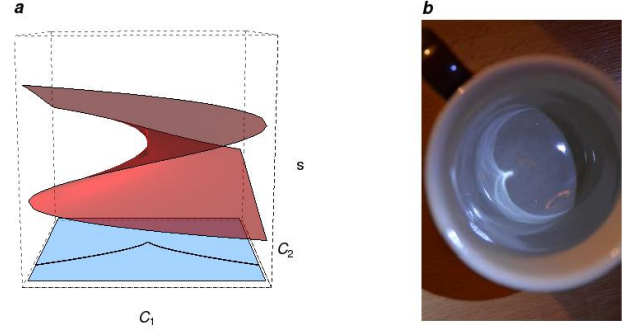


FIG. 1: The cusp catastrophe is generated by a quartic action of the form $I(s) = C_1 s + C_2 s^2 + s^4$, where (C_1, C_2) are the control parameters, and s labels the paths. Classical paths satisfy the principle of stationary action $\partial I/\partial s = 0$ which is plotted as the folded surface in (a). Under the folded section there are three classical paths reaching each point (C_1, C_2) , but two of them annihilate on the fold lines which together form a cusp $C_1 = \pm \sqrt{8/27}(-C_2)^{3/2}$ in the control plane. On the cusp the action is stationary to higher order $\partial^2 I/\partial s^2 = 0$. (b) Light reflects from the inside of a cup. Its non-parabolic shape focuses the light imperfectly forming a cusp at the base.

$\hat{H}_{\text{BH}} = U \hat{S}_z^2 - 2J \hat{S}_x$ describes a bosonic Josephson junction with on-site interaction energy U and hopping energy J . In cold atom experiments U can be tuned by a Feshbach resonance and J by the laser intensity [24].

The types of catastrophe which can occur are determined by the dimension of the control space in which the catastrophe lives. If N is conserved, Fock space is one dimensional with the discrete number difference z acting as the coordinate. Time evolution adds a second, continuous, coordinate giving a two dimensional control space. We therefore expect generic singularities to take the form of the cusp catastrophe shown in Fig. 1. The cusp is two dimensional and is the simplest catastrophe exhibiting vortices in its diffraction pattern.

Phase is an emergent quantity which becomes sharply defined in the classical limit ($N \rightarrow \infty$) as expected from $U(1)$ symmetry breaking. In the case of two coupled BECs, $\phi = \phi_1 - \phi_0$ is the phase difference between the two condensates and can be measured in an interference experiment [25]. In the same limit z becomes continuous and ϕ and z are conjugate variables. It is useful to define a semiclassical regime $N \gg 1$ and re-quantize [26] via $[\hat{\phi}, \hat{z}] = i/N$, where $1/N$ plays a role analogous to \hbar in single particle quantum mechanics, treating ϕ and z as

continuous. The significance of this regime will become clear in due course.

In the truncated Wigner approximation [27] the dynamics is treated by propagating classical solutions sampled from an initial quantum probability distribution as shown in Fig. 2. In the classical limit $\lim_{N \rightarrow \infty} H_{\text{BH}}/NJ = H_{\text{class}} = \Lambda z^2/2 - \sqrt{1-z^2} \cos \phi$ [28]. The single parameter $\Lambda = UN/2J$ fully determines the classical dynamics whereas for the quantum dynamics given below we also need to specify N . Each curve $z(t)$ in Fig. 2 is a solution of Hamilton's equations $\dot{\phi} = \partial H_{\text{class}}/\partial z$ and $\dot{z} = -\partial H_{\text{class}}/\partial \phi$ for a different value of the initial number difference z_0 , and time is scaled as $t \rightarrow Jt/\hbar$. The initial distribution we choose corresponds to a perfectly defined phase difference and hence a completely undefined number difference. Thus, the set of initial points $\{z_0\}$ is uniformly distributed over the range $-1 \leq z_0 \leq 1$ and evolves into a repeated train of cusps as seen in Fig. 2(a). These correspond to the first, or geometric, level of a catastrophe.

The precise form of the Hamiltonian will not affect the qualitative shape of any structurally stable singularities. Let us make the Hamiltonian simpler by flashing the nonlinear term on and off instantaneously at $t = 0$ and replacing $\sqrt{1-z^2}$ by unity which is valid when $|z| \ll 1$. This gives the Hamiltonian for a δ -kicked rotor $\hat{H}_{\text{kick}}/NJ = \Lambda \hat{z}^2 \delta(t)/2 - \cos \hat{\phi}$. The classical trajectories generated by H_{kick} are straight lines in the (z, t) plane and form a single cusp as shown in Figure 2(b).

In quantum theory the dynamics is generated by the application of the evolution operator to the initial state $|\psi(t)\rangle = \hat{U}(t, t_0)|\psi_0\rangle$. For \hat{H}_{kick} we find $\hat{U}(t, t_0) = \mathcal{T}\{\exp[-(i/\hbar) \int_{t_0}^t \hat{H}(t') dt']\} = \exp[i t N \cos \hat{\phi}] \exp[-i \Lambda N \hat{z}^2/2]$, where \mathcal{T} is the time ordering operator [29]. We take the initial state to be a discrete Gaussian $|\psi_0\rangle = 2^{1/4} (\frac{1}{\pi})^{3/4} \sqrt{\frac{\Lambda}{N}} \sum_{m=-N/2}^{N/2} \exp[-2(z_m \Lambda/\pi)^2] |z_m\rangle$, where $z_m = 2m/N$. The width of this state depends inversely on Λ . The Fock-space wave function is then given by

$$\begin{aligned} \psi(z_n, t) &= \langle z_n | \hat{U}(t) | \psi_0 \rangle = \left(\frac{2}{\pi}\right)^{3/4} \frac{\sqrt{\Lambda}}{N^{3/2}} \\ &\times \sum_{p, m=-N/2}^{N/2} e^{-2(\frac{\Lambda z_m}{\pi})^2} e^{-iN(\frac{\Lambda z_m^2}{2} - t \cos \phi_p - \frac{z_n - z_m}{2} \phi_p)} \end{aligned} \quad (1)$$

where $\phi_p = \frac{2\pi p}{N+1}$ is a quantized phase [30], and we have neglected an overall phase factor.

If we treat z and ϕ as continuous then the wave function can be written, in the semiclassical regime, as (Supplemental Materials)

$$\psi(z, t) \propto \int_{-\infty}^{\infty} e^{-\frac{u^2}{2\pi^2}} e^{iN\left(\frac{zu}{2} + \frac{u^2}{8\Lambda} + t \cos u\right)} du. \quad (2)$$

This can be mapped onto the Pearcey function, which is the universal diffraction integral for the cusp catastrophe,

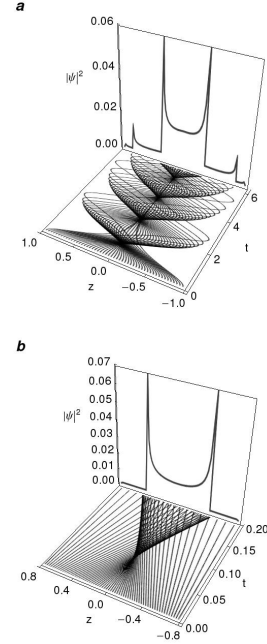


FIG. 2: Geometric cusps in Fock space as a function of time in a two mode field. The initial state has a well defined phase difference and Λ is quenched at $t = 0$. (a) The trajectories generated by the classical Bose-Hubbard Hamiltonian H_{class} form a train of cusps. (b) The kicked Hamiltonian H_{kick} generates a single cusp. The trajectories for the latter are straight lines $z(t) = -t \sin(\Lambda z_0) + z_0$. In both images $\Lambda = 4$ and the vertical back pane shows the probability density obtained by summing the trajectories arriving at each point at the final time shown.

if we expand the exponent around $\phi = u = 0$ giving

$$\begin{aligned} \psi(z, t) &\propto \int_{-\infty}^{\infty} e^{-N^{-1/2} Z(t) s^2} \\ &\times e^{i[N^{3/4} Y(z, t) s + N^{1/2} X(t) s^2 + s^4]} ds \end{aligned} \quad (3)$$

where $s = (Nt/24)^{1/4} u$, $X(t) = (\frac{1}{4\Lambda} - t) \sqrt{6/t}$, $Y(z, t) = z(3/2t)^{1/4}$ and $Z(t) = \sqrt{\frac{6}{\pi^4 t}}$. The integral consists of a Gaussian envelope multiplying the scaled Pearcey function [10] $\text{Pe}[N^{\sigma_2} X, N^{\sigma_1} Y] = \int_{-\infty}^{\infty} e^{i(N^{\sigma_1} Y s + N^{\sigma_2} X s^2 + s^4)} ds$, where we have identified the Berry indices ($\sigma_2 = 1/2, \sigma_1 = 3/4$) which govern the scaling of fringe spacings (and therefore distances) in the (X, Y) -plane. The Pearcey function can be recognized as the Feynman path integral representation of the cusp wave function as its exponent contains the normal form of the scaled action function $I(s; N)$ for the cusp. The geometric caustics are independent of N and fixed in the (z, t) -plane. Varying N only changes the wavelength of the interfering waves making it easier to highlight the effect of second quantization.

Fig. 3 shows the probability amplitude and the phase

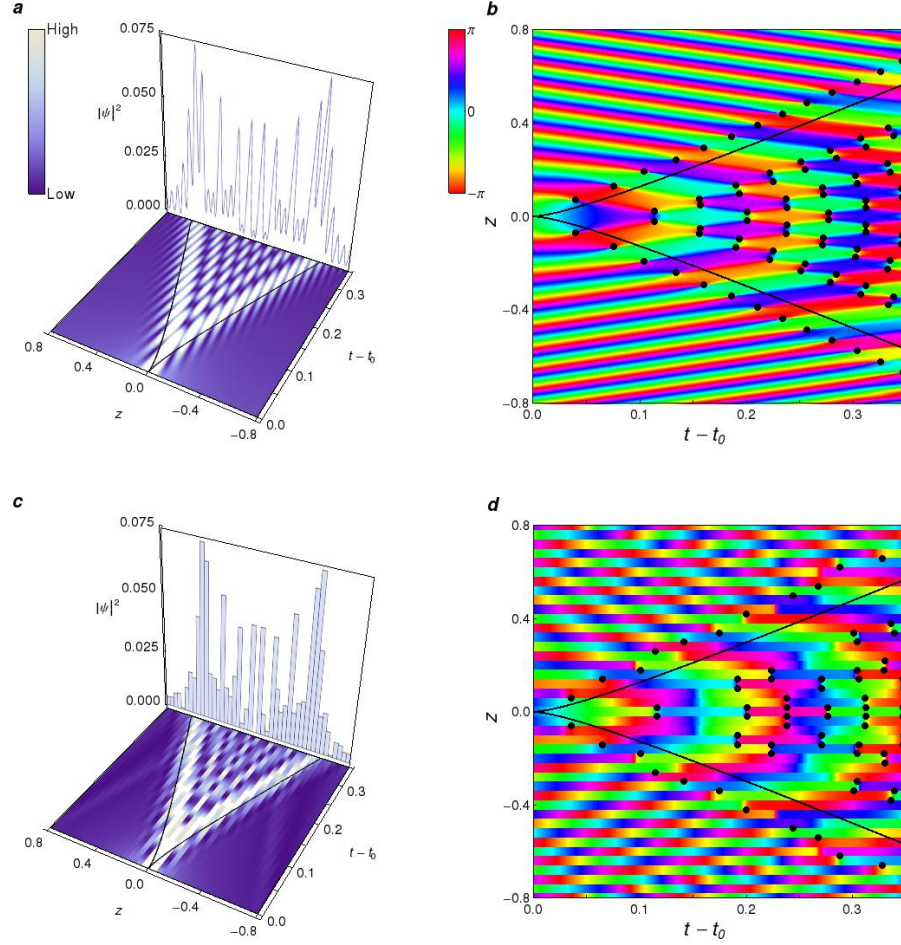


FIG. 3: Cusps and vortices in the wave (top row) and second-quantized (bottom row) theories. Panel (a) shows a density plot of the probability amplitude computed by the wave function given in Eq. (2). In contrast to Fig. 2(b), the wave function allows for interference, so the inside of the cusp is filled with light and dark regions where there is constructive and destructive interference, respectively. Panel (b) plots the phase of the wave function given in Eq. (2) where the black circles mark the locations of vortices. The black curves give the fold lines of the geometric caustics given by the condition $\partial I/\partial s = \partial^2 I/\partial s^2 = 0$. In these images the cores of the vortices are identified by the termination point of curves of constant phase. Panels (c) and (d) are the second-quantized versions of (a) and (b), respectively, and are given by exact diagonalization of \hat{H}_{kick} . Here, the probability amplitude and phase cannot be distinguished beyond the emergent quantization length, $1/N$, resulting in some vortices missing in the quantized space. All images were generated for $N = 50$ and $\Lambda = 2.1$.

of both the semiclassical and discrete cusps for $N = 50$, $\Lambda = 2.1$. The discrete cusp (bottom row) was generated by numerically solving the Schrödinger equation $i\hbar\partial_t|\psi\rangle = \hat{H}_{\text{kick}}|\psi\rangle$ and the semiclassical cusp (top row) was generated using Eq. (2). Starting with the semiclassical cusp in Fig. 3(a) we see a detailed interference pattern within the cusp where the centers of the darkest regions are points where the amplitude is exactly zero and are dislocations (vortex cores). This means if our wave function is given by $\psi = \rho e^{i\theta}$, then an infinitesimal circuit enclosing the vortex gives $\oint d\theta = \pm 2\pi$. Panel (c) shows the second-quantized analogue of (a) where we see the location of the cores is no longer obvious because they have been smoothed out over the quantization length, $1/N$. However, hints of them remain because we still get

circuits summing to $\pm 2\pi$ only now the circuits are no longer infinitesimal because they can't be smaller than $1/N$. The result of the discretization is z is chopped up into bands and resembles a discrete sampling of (a). Taking a closer look at the vortex structure, panels (b) and (d) show the phases of their respective wave functions where the black dots mark locations of vortices. In comparing the two, the vortex network is more rigid in the second-quantized case because when a vortex is detected we put a black dot between two bands. We do this because it is the most democratic spot to mark the location of a vortex given that we don't know exactly where its core is. This results in every pair having the same size whereas in the continuous case the pairs vary in size depending on where they are in the plane.

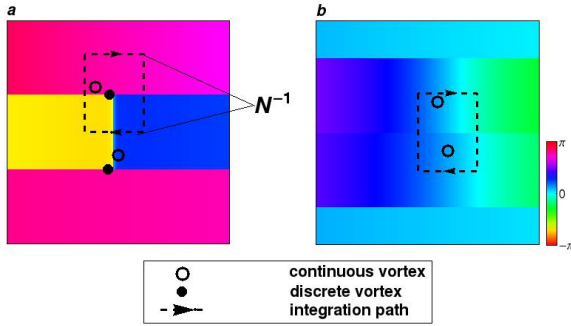


FIG. 4: Magnified regions of Fig. 3d. Panel (a) shows a region where a quantized vortex and anti-vortex pair (filled circles) is detected as well as the corresponding semiclassical pair (unfilled circles) from Fig. 3b. The dashed black box with arrows shows a typical integration path; exaggerated in the time (horizontal) direction, but exact in the transverse direction due to the minimum length scale, $1/N$. When a single semiclassical vortex is enveloped by the integration path it can be distinguished in the quantized space and we detect it. However, as we see in panel (b) when both members of a semiclassical pair are enveloped they can't be distinguished. The result in the quantized space is the pair effectively annihilate each other.

The most striking feature of the discretization is the missing vortex pairs in Fig. 3(d) because in the Pearcey case the vortices never vanish for finite N . To understand this we look at Fig. 4 which shows magnified regions of Fig. 3(d) highlighting both present and missing discrete vortex pairs. The filled and unfilled circles mark the locations of the quantized vortices and their corresponding semiclassical vortices from Fig. 3(b), respectively. The dashed rectangle with arrows represents the integration path used to find the vortices in the quantized space; exaggerated in the time (horizontal) direction, but exact in the z (vertical) direction with length, $1/N$. The important thing to notice is that when the integration path encompasses one semiclassical vortex (unfilled circle) it can be resolved and we also find a quantum vortex (filled circle) as shown in Fig. 4(a). However, when the path encompasses both members of a semiclassical pair we cannot distinguish between each member and they cancel each other out resulting in no second-quantized pair being detected. Therefore, due to the discrete nature of Fock space we lack the resolution to see some vortex pairs because they have effectively annihilated each other.

The vortex resolution can be shown by comparing the relevant length scales of the system. The first is the Bragg angle spacing, θ_B , which for wavenumber k and

lattice periodicity a is $1/ka$. For us $k = N$ and $a = \pi/\Lambda$, so $\theta_B \propto \Lambda/N$. The second is the transverse distance between vortices of the same pair which we find to be $d_v \propto (t/N^3)^{1/4}$ from equation (3) for large N . We define our resolution parameter as

$$\mathcal{R} = d_v/\theta_B \propto \frac{(tN)^{1/4}}{\Lambda} \quad (4)$$

where we require $\mathcal{R} \gg 1$ in order to see each individual vortex. Due to the dependencies of \mathcal{R} on t and Λ and its weak dependence on N there is a wide range of system sizes where the phenomena of vanishing vortices can be detected. In generating Figs. 3a,b we sampled z in Eq. (2) in segments of size $\frac{1}{10N}$, so the resolution was ten times greater than Figs. 3c,d. Thus, according to \mathcal{R} we would need $N = 5 \times 10^5$ particles in the system to achieve the same semiclassical images.

Discussion Quantum catastrophes are the structurally stable singularities of quantum fields and represent a new generation of catastrophe theory. They live in Fock space and are naturally discrete, diverging in the classical limit $N \rightarrow \infty$. Quantum catastrophes can be mapped onto classical wave catastrophes at finite excitation number N if we treat Fock space as continuous. However, the mapping is imperfect as some of fine dislocation structure present in wave catastrophes is removed by the discretization. Wave catastrophes, which are continuous, obey a remarkable set of self-similar scaling relations determined by the Arnold and Berry exponents. This classical scaling is violated in quantum catastrophes due to the fundamental discretization of Fock space and can therefore be viewed as a type of quantum anomaly.

I. METHODS

To find the locations of vortices we divided the (z, t) -plane into segments in both z and t . In the continuous case the segments had dimensions $\Delta z = 0.1/N$, $\Delta t = 0.001$ and in the discrete case had dimensions $\Delta z = 1/N$, $\Delta t = 0.001$. Next, defining the phase of a given segment by $\theta_{i,j} = \theta(i\Delta t, j\Delta z)$ where $i = 0, 1, \dots, 350$ and $j = -1/\Delta z, -1/\Delta z + 1, \dots, 1/\Delta z - 1, 1/\Delta z$ we summed the difference in phase between adjacent segments forming a loop consisting of a rectangle of four segments. Our conventions in summing the phase were that we go clockwise around each loop and that the phase be mapped to a cylinder in the range $-\pi < \theta < \pi$. When our sum was approximately $\pm 2\pi$ we put a black dot at the center of the rectangle.

[1] R. Thom, *Structural Stability and Morphogenesis* (Benjamin, Reading MA, 1975).

[2] J. F. Nye, *Natural focusing and the fine structure of light* (Institute of Physics, Philadelphia, 1999).

- [3] M. V. Berry, J. Phys. A: Math. Gen. **10**, 2061 (1977).
- [4] R. Höhmann, U. Kuhl, H.-J. Stöckmann, L. Kaplan, and E. J. Heller, Phys. Rev. Lett. **104**, 093901 (2010).
- [5] V. I. Arnold, S. F. Shandarin and Ya. B. Zeldovich, Geophys. Astrophys. Fluid Dynamics **20**, 111 (1982).
- [6] V. I. Arnol'd, Russ. Math. Survs. **20**, 1 (1975).
- [7] M. V. Berry, Adv. Phys. **25**, 1 (1976).
- [8] H. Trinkhaus and F. Drepper, J. Phys. A **10**, L11 (1977).
- [9] Chapter 36 of *NIST Handbook of Mathematical Functions*, edited by Olver et al. (Cambridge University, New York, 2010).
- [10] T. Pearcey, Phil. Mag. **37**, 311 (1946).
- [11] J. F. Nye and M. V. Berry, Proc. R. Soc. Lond. A **336**, 165 (1974).
- [12] U. Leonhardt, Nature **415**, 406 (2002).
- [13] M. V. Berry and M. R. Dennis, J. Opt. A: Pure Appl. Opt. **6**, S178 (2004).
- [14] M. V. Berry, Nonlinearity **21**, T19 (2008).
- [15] D. H. J. O'Dell, Phys. Rev. Lett. **109**, 150406 (2012).
- [16] A. Luis, Phys. Rev. A **66**, 013806 (2002).
- [17] N. Korolkova and R. Loudon, Phys. Rev. A **71**, 032343 (2005).
- [18] H. J. Lipkin, N. Meshkov and A. J. Glick, Nuclear Phys. **62**, 188 (1965).
- [19] A. Das, K. Sengupta, D. Sen, and B. K. Chakrabarti, Phys. Rev. B **74**, 144423 (2006).
- [20] M. Albiez, R. Gati, J. Fölling, S. Hunsmann, M. Cristiani, and M. K. Oberthaler, Phys. Rev. Lett. **95**, 010402 (2005).
- [21] S. Levy, E. Lahoud, I. Shomroni, and J. Steinhauer, Nature **449**, 579 (2007).
- [22] A. Trenkwalder, G. Spagnolli, G. Semeghini, S. Coop, M. Landini, P. Castilho, L. Pezzè, G. Modugno, M. Inguscio, A. Smerzi and M. Fattori, Nat. Phys. **12**, 826 (2016).
- [23] G. J. Milburn, J. Corney, E. M. Wright, and D. F. Walls, Phys. Rev. A **55**, 4318 (1997).
- [24] T. Zibold, E. Nicklas, C. Gross, and M. K. Oberthaler, Phys. Rev. Lett. **105**, 204101 (2010).
- [25] M. R. Andrews, C. G. Townsend, H.-J. Miesner, D. S. Durfee, D. M. Kurn, W. Ketterle, Science **275**, 637 (1997).
- [26] A. J. Leggett *Chance and Matter* (Les Houches 1986, Session XLVI) ed J. Souletie et al (North-Holland, Amsterdam, 1987).
- [27] J. Javanainen and J. Ruostekoski, New J. Phys. **15**, 013005 (2013).
- [28] A. Smerzi, S. Fantoni, S. Giovanazzi, and S. R. Shenoy, Phys. Rev. Lett. **79**, 4950 (1997).
- [29] F. Haake, *Quantum Signatures of Chaos*, 3rd edition (Springer, Berlin, 2009).
- [30] D. T. Pegg and S. M. Barnett, Phys. Rev. A, **39**, 1665 (1989).